SUPPLEMENTAL INFORMATION

The New York Presbyterian (NYP) COVID-19 cohort was a cohort of study subjects who presented to New York Presbyterian Weill Cornell Medicine Center and New York Presbyterian Lower Manhattan Hospital between March and May 2020. The baseline characteristics of this cohort, including comorbidities at presentation and stratified according to clinical outcome, are described in **Supplementary Table 1**.

SUPPLEMENTAL METHODS

Mass spectrometry. Excised bands were digested in-gel with trypsin overnight at 37°C following reduction with 5mM dithiothreitol (DTT) and 14mM alkylation with iodoacetamide. The digests were vacuum centrifuged to near dryness and desalted by micro-C18 columns. A ThermoFisher Scientific EASY-nLC 1000 coupled on-line to a Fusion Lumos mass spectrometer (Thermo Fisher Scientific) and 75 µm x 15 cm chromatography columns (ReproSil-Pur C18-AQ, 3 µm, Dr. Maisch GmbH, German) packed in-house were used for peptides separation. Peptides were separated with a gradient of 3–30% buffer B over 50 min, 30%-80% B over 10 min at a flow rate of 300 nL/min. The Fusion Lumos mass spectrometer was operated in data dependent mode. Full MS scans were acquired in the Orbitrap mass analyzer over a range of 300-1500 m/z with resolution 60,000. The top 15 most abundant precursors with charge states between 2 and 5 were selected with an isolation window of 1.4 m/z by the quadrupole and fragmented by higher-energy collisional dissociation with normalized collision energy of 35. MS/MS scans were acquired in the Orbitrap mass analyzer with resolution 15,000. The automatic gain control target value was 1e6 for full scans and 5e4 for MS/MS scans respectively, and the maximum ion injection time is 60 ms for both.

The raw files were processed using the MaxQuant computational proteomics platform Version 1.6.17.0 (Max Planck Institute, Munich, Germany) for protein identification. The fragmentation spectra were used to search the UniProt human protein database (downloaded on

09/21/2017). Oxidation of methionine and protein N-terminal acetylation were used as variable modifications for database searching. The precursor and fragment mass tolerances were set to 7 and 20 ppm, respectively. Both peptide and protein identifications were filtered at 1% false discovery rate based on decoy search using a database with the protein sequences reversed.

Supplementary Table 1. Baseline Characteristics of NYP COVID-19 Cohort by Outcome.

*Parameter	Intubation/Death (n=157)	Intubation/Discharge (n=249)	No Intubation/Discharge (n=965)	**p-value
Sex n (%)				<0.001
Female	42 (27%)	83 (33%)	413 (43%)	
Male	115 (73%)	166 (67%)	552 (57%)	
Age [IQI]	71 [63, 78]	61 [50, 70]	61 [49, 71]	<0.001
Race n (%)				<0.001
Asian	41 (26%)	45 (18%)	144 (15%)	
Black	14 (8.9%)	20 (8.0%)	157 (16%)	
Hispanic	37 (24%)	72 (29%)	230 (24%)	
White	44 (28%)	61 (24%)	257 (27%)	
BMI [IQI]	27 [23, 31]	29 [26,33]	27 [24,31]	<0.001
Hypertension n (%)	100 (64%)	135 (54%)	490 (51%)	0.010
Diabetes n (%)	59 (38%)	83 (33%)	279 (29%)	0.056
Coronary Artery Disease n (%)	42 (27%)	29 (12%)	110 (11%)	<0.001
COPD n (%)	15 (9.6%)	13 (5.2 %)	25 (2.6%)	<0.001
Active Cancer n (%)	14 (8.9%)	8 (3.2%)	55 (5.7%)	0.051
Supplemental Oxygen in 1st 3 Hours n (%)	135 (86%)	195 (78%)	390 (40%)	<0.001

*Statistics presented: N (%); median [IQI]
**Tests used: Pearson's Chi-squared test; Kruskal-Wallis rank sum test; Fisher's exact test; Fisher's exact test with Monte Carlo simulated p-value

SUPPLEMENTARY FIGURE LEGENDS

Supplementary Figure 1. Ferritin parameters in patients with COVID-19 ARDS. (**A**) Flow diagram of the NYP COVID-19 Cohort. (**B**) Schematic illustrating the calculation of delta ferritin in subjects in the NYP COVID-19 cohort (n=343), with red circles representing first serum ferritin measurement available during hospital admission and green circles last serum ferritin measurement prior to 21 days admission, death, or hospital discharge, whichever is later.

Supplementary Figure 2. Monocyte *FTL* expression across COVID-19 severity. (**A**) Violin plots of CD14+ Monocytes of *FTL* expression by donor cells across increasing covid severity. P-values calculated by Kruskal-Wallis test. ****p<0.0001. (**B**) Peripheral blood mononuclear cell (PBMC) expression of *FTH1* in the NYP COVID-19 cohort, displayed as violin plots with solid line indicating the median expression and dashed lines indicating the upper and lower quartiles, with p-value by unpaired Student's t-test. (**C**) *Ftl* Transcripts per Million (TPM) from bulk RNA-Seq of BAL cells following intratracheal LPS instillation, presented as mean ± SEM with p-value by unpaired Student's t-test, *p<0.05.

Supplementary Figure 3. Hyperoxia induces macrophage gene expression changes. (**A**) Volcano plot highlighting gene expression (n=3 for both groups) changes comparing BMDMs from *Fth1*$^{fl/fl}$ mice exposed to 96 hours of hyperoxia compared to those from room air (RA) *Fth1*$^{fl/fl}$ mice, using a cut-off of 1.25 fold-change and false discovery rate (FDR) less than 0.05, illustrated using VolcaNoseR. (**B**) Gene ontology (biological process) analysis of upregulated genes in BMDMs from mice exposed to hyperoxia relative to those from RA mice.

Supplementary Figure 4. Murine LysM-Cre targeted FTH1 deletion. (**A**) Breeding scheme for myeloid FTH1-deficient (*Fth1*$^{\Delta LysM}$) mice, created using biorender. Real-time polymerase chain reaction (RT-PCR) of BMDM *Fth1* (**B**, n=3 for *Fth1*$^{fl/fl}$, n=3 for *Fth1*$^{\Delta LysM}$) and AM *Fth1* (**C**, n=2 for

Fth1$^{fl/fl}$, n=3 for *Fth1*$^{\Delta LysM}$). Data presented as mean ± SEM with p-value by unpaired Student's t-test, *p<0.05, **p<0.01, ****P<0.0001. (**D**) Representative immunoblot of FTH1 protein expression in bone marrow-derived macrophages (BMDMs) from *Fth1*$^{fl/fl}$ (n=3) and *Fth1*$^{\Delta LysM}$ (n=3) mice.

Supplementary Figure 5. Cd11c-Cre driven FTH1 deletion protects against hyperoxia. (**A**) BALF total cell count and (**B**) macrophages and monocytes in *Fth1*$^{fl/fl}$ and *Fth1*$^{\Delta Cd11c}$ mice in room air and hyperoxia conditions. P-values by 2-way analysis of variance (ANOVA) with Šídák's correction for multiple comparisons. *p<0.05, **, o<0.01, ****p<0.0001.

Supplementary Figure 6. Decreased BAL immune cells in *Fth1*$^{fl/fl}$ mice are not due to decreased chemokine signaling. BALF MCP-3 (**A**, n=3/7/6 for *Fth1*$^{fl/fl}$ mice and n=3/7/7 for *Fth1*$^{\Delta LysM}$ mice at the room air/72hr/96hr time points) and MCP-5 (**B**, n=4/8/10 for *Fth1*$^{fl/fl}$ mice and n=5/6/7 for *Fth1*$^{\Delta LysM}$ mice at the room air/72hr/96hr time points), presented as mean ± SEM with p-values by 2-way analysis of variance (ANOVA) with Šídák's correction for multiple comparisons. *p<0.05, ***, P<0.001.

Supplementary Figure 7. FTH1 depletion upregulates pathways involved in glutathione metabolism and protection against ferroptosis. (**A**) Volcano plot highlighting gene expression (n=3 for both groups) changes comparing BMDMs from *Fth1*$^{\Delta LysM}$ mice to those from *Fth1*$^{fl/fl}$ mice at room air, using a cut-off of 1.25 fold-change and false discovery rate (FDR) less than 0.05, illustrated using VolcaNoseR. Upregulated genes in BMDMs from *Fth1*$^{\Delta LysM}$ mice relative to BMDMs from *Fth1*$^{fl/fl}$ mice, analyzed using Gene Ontology (**B**) Biological Process and (**C**) KEGG are illustrated using ShinyGo. (**D**) Gene ontology (biological process) and (**E**) KEGG analysis of upregulated genes in BMDMs from *Fth1*$^{\Delta LysM}$ mice exposed to 96 hours of hyperoxia relative to those from *Fth1*$^{fl/fl}$ mice exposed to 96 hours of hyperoxia.

Supplementary Figure 8. Deferiprone lowers macrophage total iron levels. Total iron as measured by graphite furnace atomic absorption spectrometry (GFAAS) in fetal liver-derived macrophages (FLAMs) treated with 24 hours of 100 μM of deferiprone (DFP) relative to control macrophages. Data presented mean ± SEM with p-value by unpaired Student's t test, ***p<0.001.

Supplementary Figure 9. Alveolar macrophage (AM) NCOA4 depletion alters AM iron metabolism and cellular response to hyperoxia. (**A**) Representative immunoblot of NCOA4 protein expression in bone marrow-derived macrophages (BMDMs) from *Fth1*$^{fl/fl}$ (n=3) and *Fth1*$^{\Delta LysM}$ (n=3) mice; same membrane re-blotted as **Figure 3B**. Real-time polymerase chain reaction (RT-PCR) of AM *Ncoa4* (**B**, n=10 for *Ncoa4*$^{fl/fl}$, n=7 for *Ncoa4*$^{\Delta Cd11c}$), *Fth1* (**C**, n=8 for *Ncoa4*$^{fl/fl}$, n=5 for *Ncoa4*$^{\Delta Cd11c}$) and *Tfrc* (**D**, n=8 for *Ncoa4*$^{fl/fl}$, n=8 for *Ncoa4*$^{\Delta Cd11c}$) mRNA expression. (**E**) Total iron content in AMs from *Ncoa4*$^{fl/fl}$ and *Ncoa4*$^{\Delta Cd11c}$ mice, normalized to total protein. BALF macrophages/monocytes (**F**) and neutrophil count (**G**) in *Ncoa4*$^{fl/fl}$ and *Ncoa4*$^{\Delta Cd11c}$ mice under RA and hyperoxia conditions. Data (B-G) presented mean ± SEM with p-values by unpaired Student's t-test (B-E) or 2-way analysis of variance (ANOVA) with Šídák's correction (F-G) for multiple comparisons. **p<0.01, ****P<0.0001.

Supplementary Figure 10. Serum ferritin in human ARDS is enriched for FTL. (**A**) Representative native electrophoresis gel image from native serum ferritin isolation, with quantification of FTL and FTH1 by mass spectrometry. (**B**) Relative percentage of FTL or FTH1 subunits.

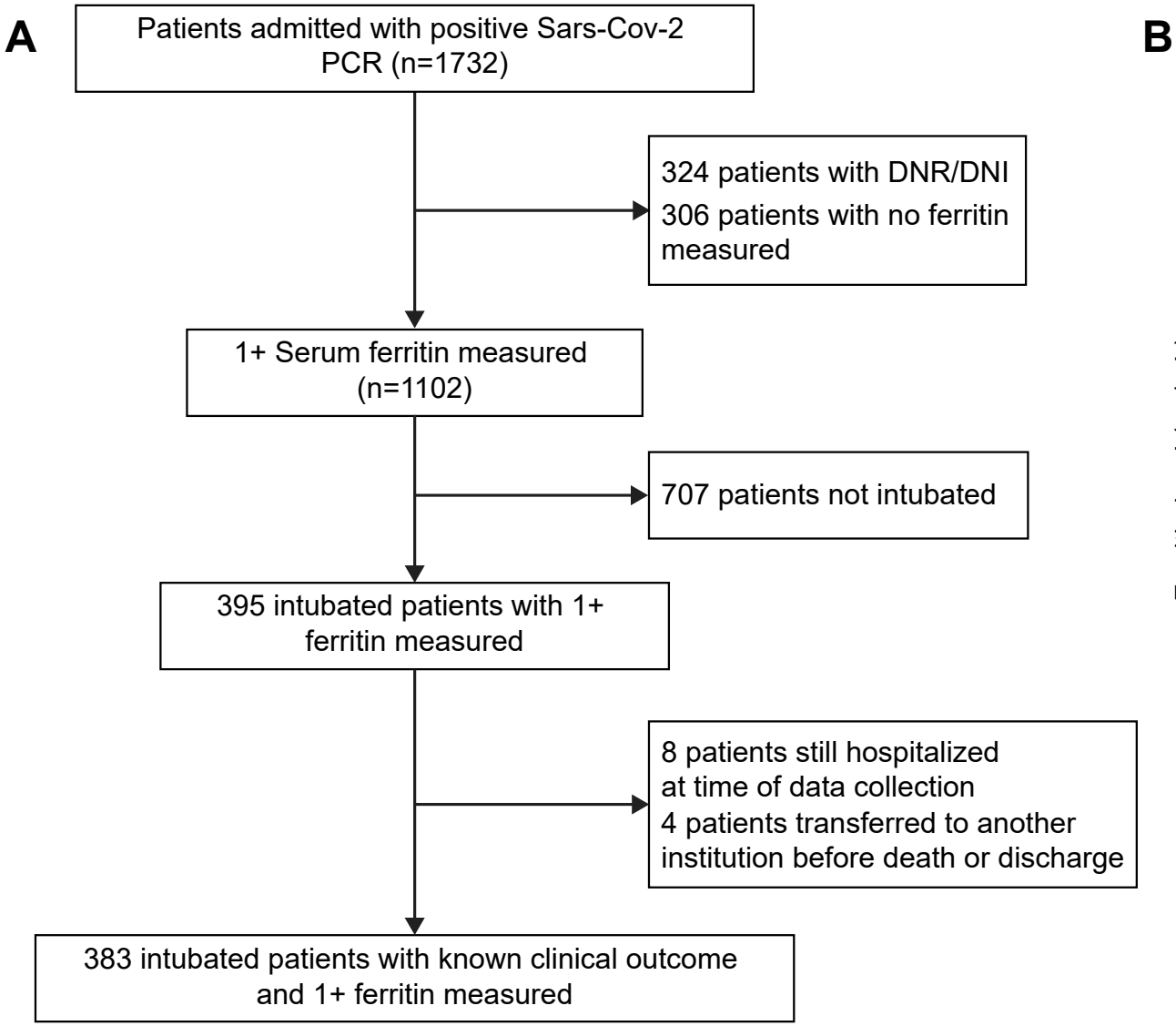

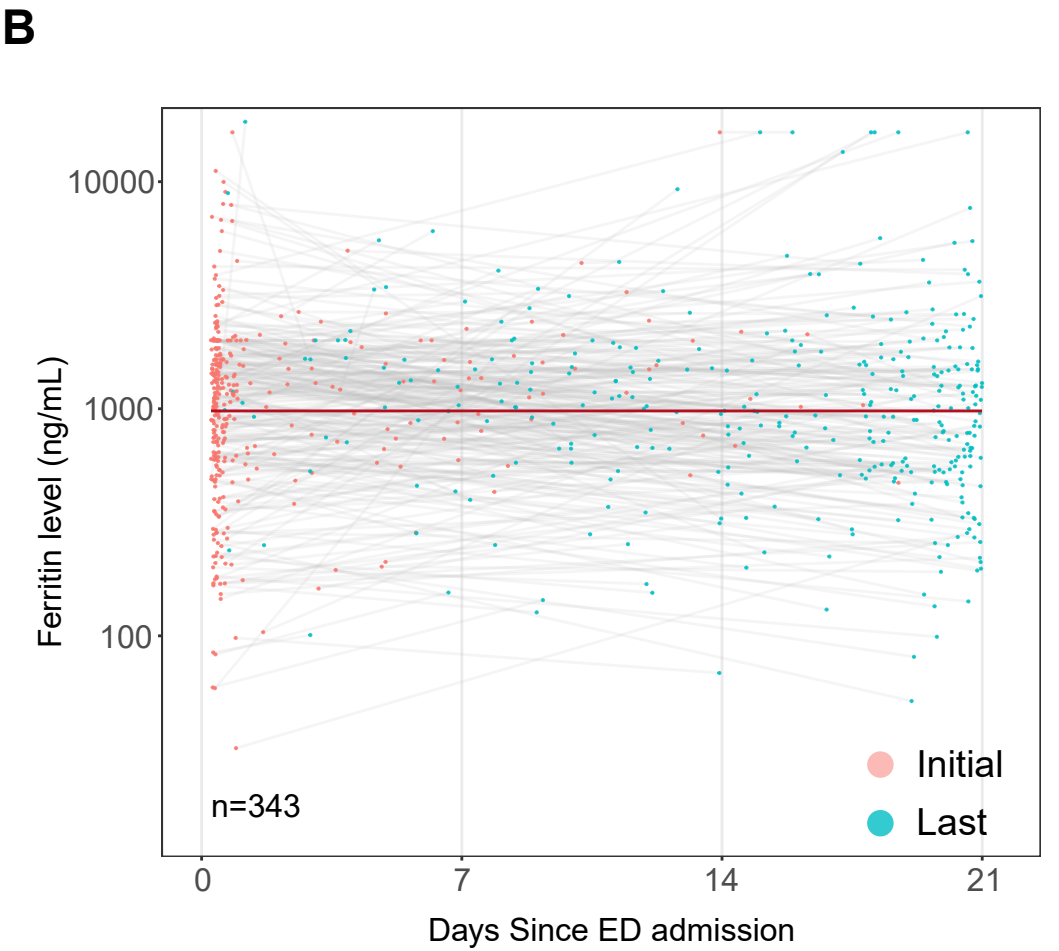

Supplementary Figure 1

Supplementary Figure 1. Ferritin parameters in patients with COVID-19 ARDS. (**A**) Flow diagram of the NYP COVID-19 Cohort. (**B**) Schematic illustrating the calculation of delta ferritin in subjects in the NYP COVID-19 cohort (n=343), with red circles representing first serum ferritin measurement available during hospital admission and green circles last serum ferritin measurement prior to 21 days admission, death, or hospital discharge, whichever is later.

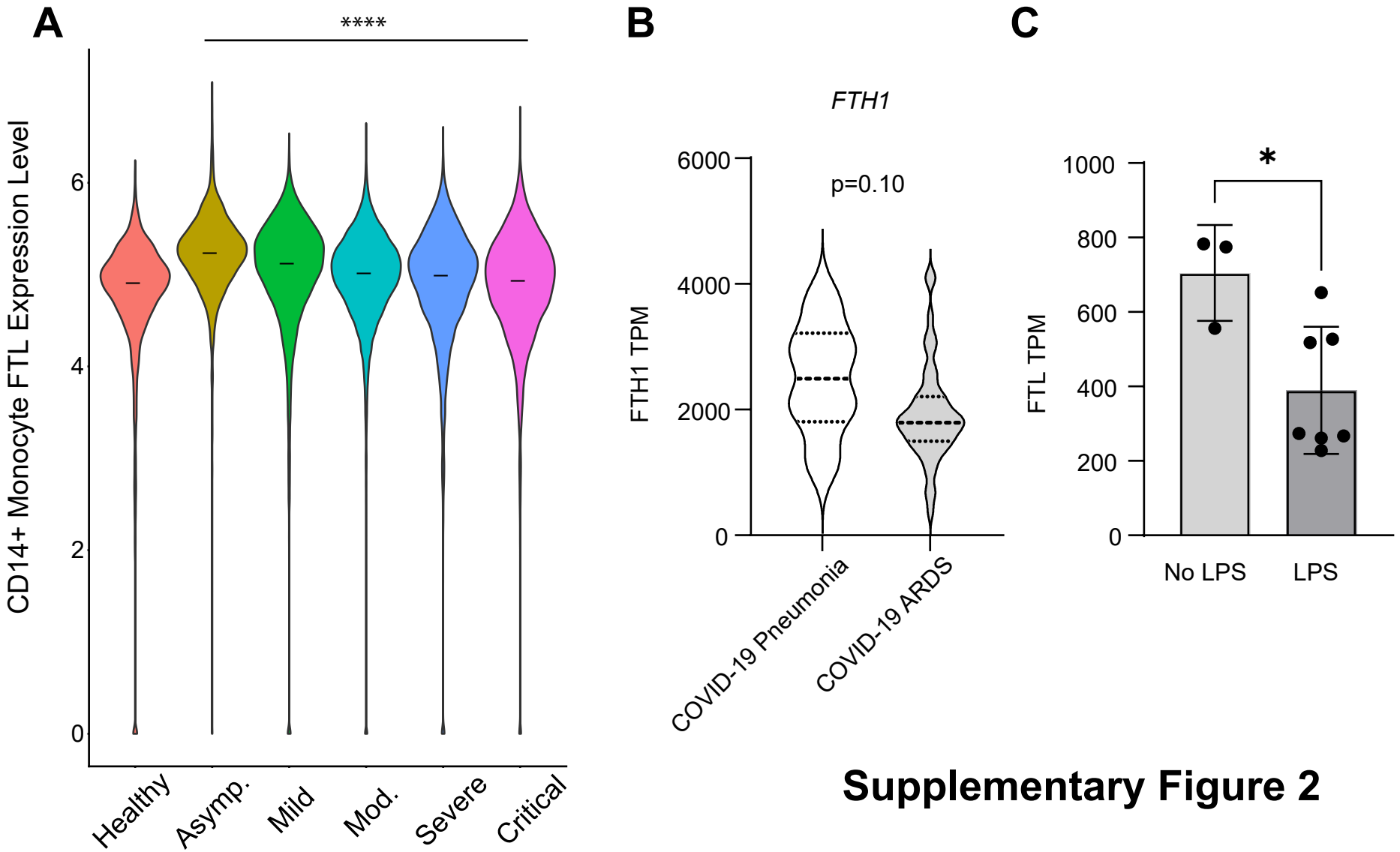

Supplementary Figure 2

Supplementary Figure 2. Monocyte FTL expression across COVID-19 severity. (**A**) Violin plots of CD14+ Monocytes of *FTL* expression by donor cells across increasing covid severity. P-values calculated by Kruskal-Wallis test. ****p<0.0001. (**B**) Peripheral blood mononuclear cell (PBMC) expression of *FTH1* in the NYP COVID-19 cohort, displayed as violin plots with solid line indicating the median expression and dashed lines indicating the upper and lower quartiles, with p-value by unpaired Student's t-test. (**C**) *Ftl* Transcripts per Million (TPM) from bulk RNA-Seq of BAL cells following intratracheal LPS instillation, presented as mean ± SEM with p-value by unpaired Student's t-test, *p<0.05.

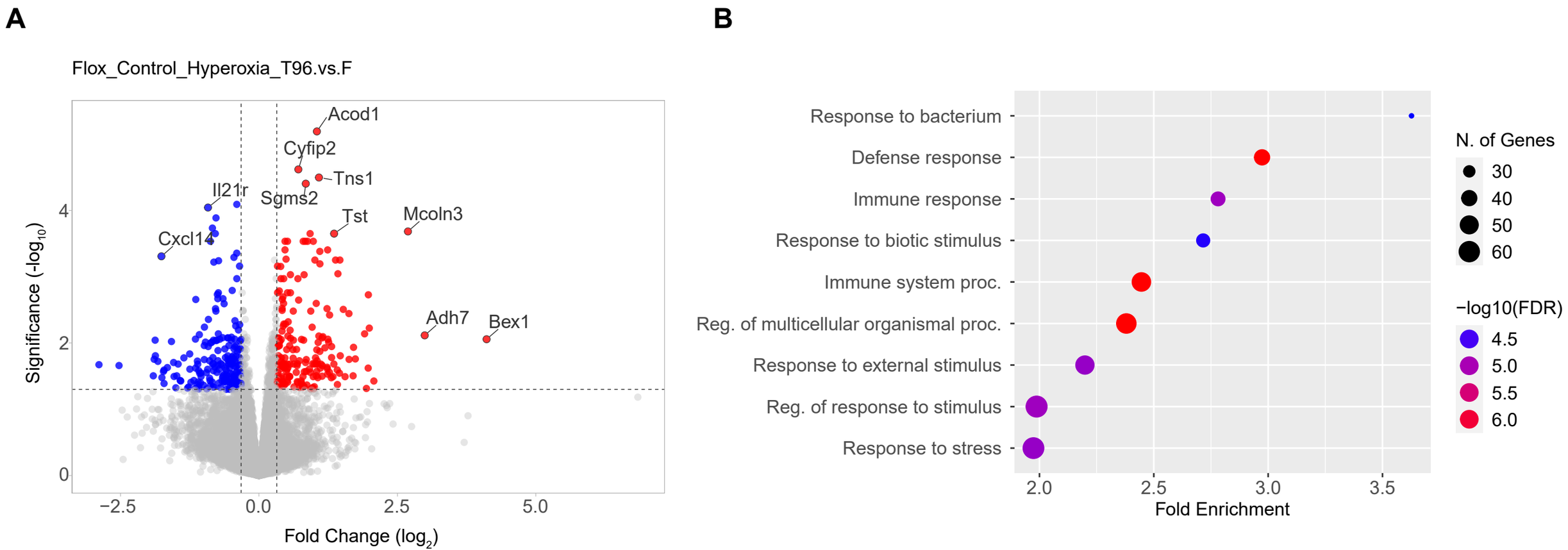

Supplementary Figure 3

Supplementary Figure 3. Hyperoxia induces macrophage gene expression changes. (**A**) Volcano plot highlighting gene expression (n=3 for both groups) changes comparing BMDMs from *Fth1*$^{fl/fl}$ mice exposed to 96 hours of hyperoxia compared to those from room air (RA) *Fth1*$^{fl/fl}$ mice, using a cut-off of 1.25 fold-change and false discovery rate (FDR) less than 0.05, illustrated using VolcaNoseR. (**B**) Gene ontology (biological process) analysis of upregulated genes in BMDMs from mice exposed to hyperoxia relative to those from RA mice.

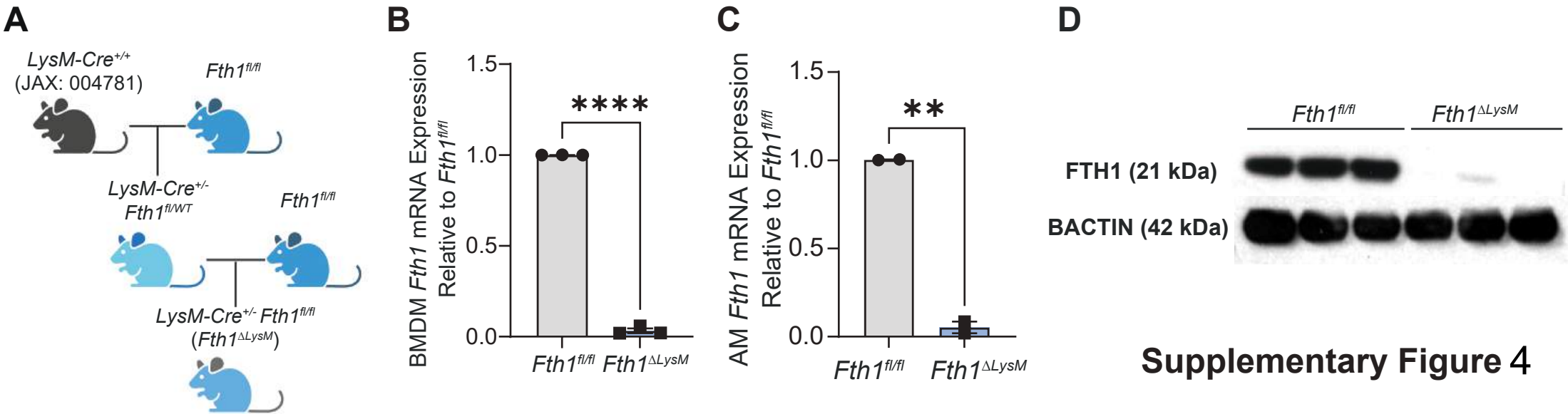

Supplementary Figure 4. Murine LysM-Cre targeted FTH1 deletion. (**A**) Breeding scheme for myeloid FTH1-deficient (*Fth1*$^{\Delta LysM}$) mice, created using biorender. Real-time polymerase chain reaction (RT-PCR) of BMDM *Fth1* (**B**, n=3 for *Fth1*$^{fl/fl}$, n=3 for *Fth1*$^{\Delta LysM}$) and AM *Fth1* (**C**, n=2 for *Fth1*$^{fl/fl}$, n=3 for *Fth1*$^{\Delta LysM}$). Data presented as mean ± SEM with p-value by unpaired Student's t-test, *p<0.05, **p<0.01, ****P<0.0001. (**D**) Representative immunoblot of FTH1 protein expression in bone marrow-derived macrophages (BMDMs) from *Fth1*$^{fl/fl}$ (n=3) and *Fth1*$^{\Delta LysM}$ (n=3) mice.

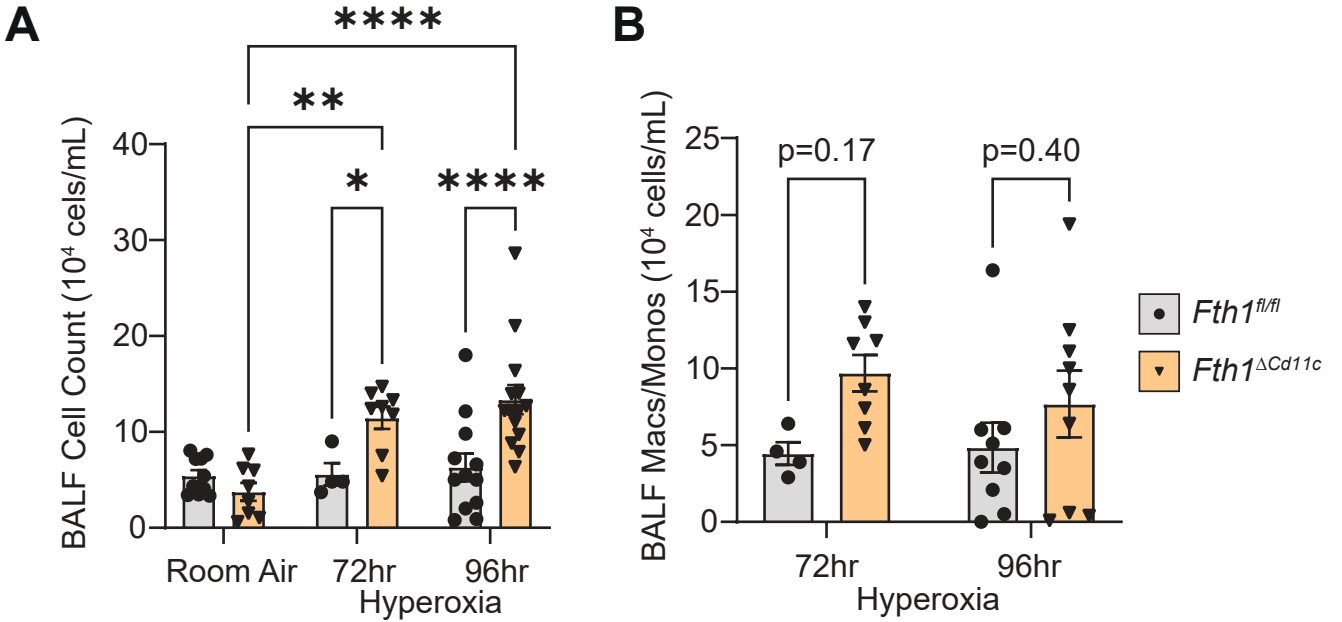

Supplementary Figure 5

Supplementary Figure 5. Cd11c-Cre driven FTH1 deletion protects against hyperoxia. (**A**) BALF total cell count and (**B**) macrophages and monocytes in *Fth1*$^{fl/fl}$ and *Fth1*$^{\Delta Cd11c}$ mice in room air and hyperoxia conditions. P-values by 2-way analysis of variance (ANOVA) with Šídák's correction for multiple comparisons. *p<0.05, **, o<0.01, ****p<0.0001.

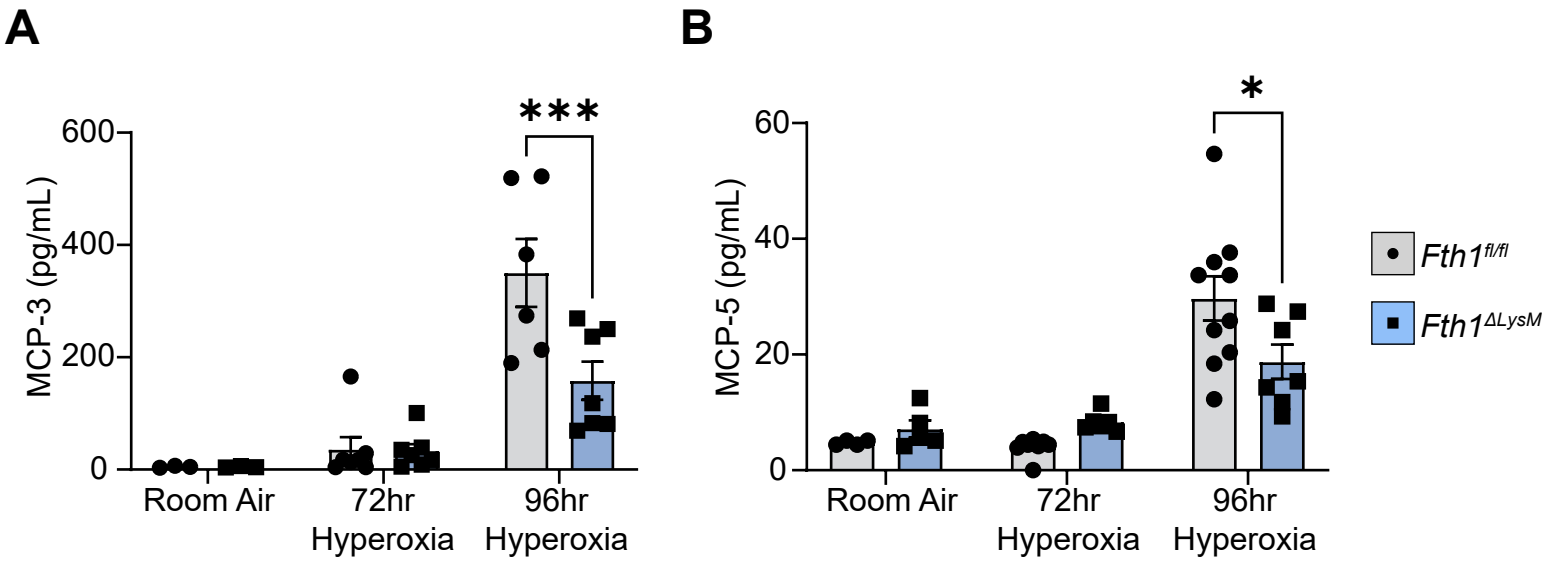

Supplementary Figure 6

Supplementary Figure 6. Decreased BAL immune cells in *Fth1$^{fl/fl}$* mice are not due to decreased chemokine signaling. BALF MCP-3 (**A**, n=3/7/6 for *Fth1$^{fl/fl}$* mice and n=3/7/7 for *Fth1$^{\Delta LysM}$* mice at the room air/72hr/96hr time points) and MCP-5 (**B**, n=4/8/10 for *Fth1$^{fl/fl}$* mice and n=5/6/7 for *Fth1$^{\Delta LysM}$* mice at the room air/72hr/96hr time points), presented as mean ± SEM with p-values by 2-way analysis of variance (ANOVA) with Šídák's correction for multiple comparisons. *p<0.05, ***, P<0.001.

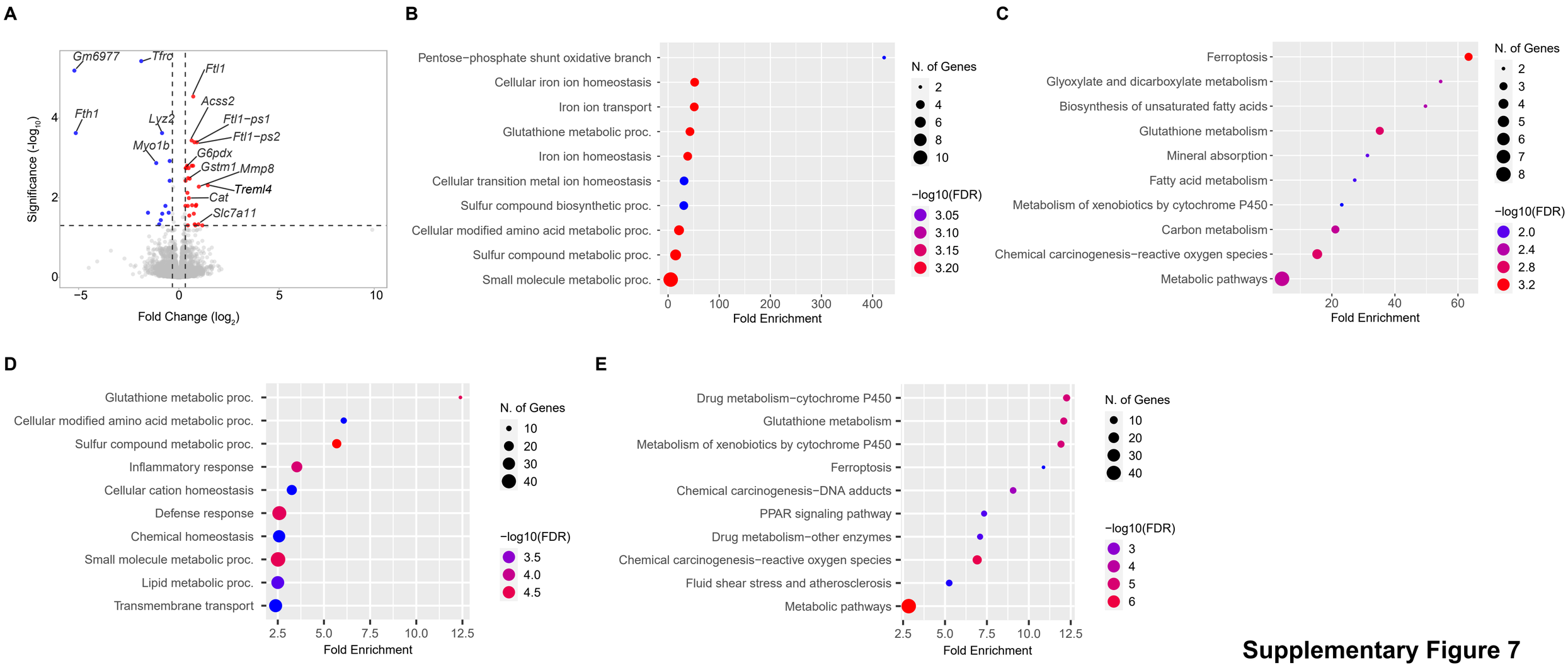

Supplementary Figure 7

Supplementary Figure 7. FTH1 depletion upregulates pathways involved in glutathione metabolism and protection against ferroptosis. (**A**) Volcano plot highlighting gene expression (n=3 for both groups) changes comparing BMDMs from *Fth1*$^{\Delta LysM}$ mice to those from *Fth1*$^{fl/fl}$ mice at room air, using a cut-off of 1.25 fold-change and false discovery rate (FDR) less than 0.05, illustrated using VolcaNoseR. Upregulated genes in BMDMs from *Fth1*$^{\Delta LysM}$ mice relative to BMDMs from *Fth1*$^{fl/fl}$ mice, analyzed using Gene Ontology (**B**) Biological Process and (**C**) KEGG are illustrated using ShinyGo. (**D**) Gene ontology (biological process) and (**E**) KEGG analysis of upregulated genes in BMDMs from *Fth1*$^{\Delta LysM}$ mice exposed to 96 hours of hyperoxia relative to those from *Fth1*$^{fl/fl}$ mice exposed to 96 hours of hyperoxia.

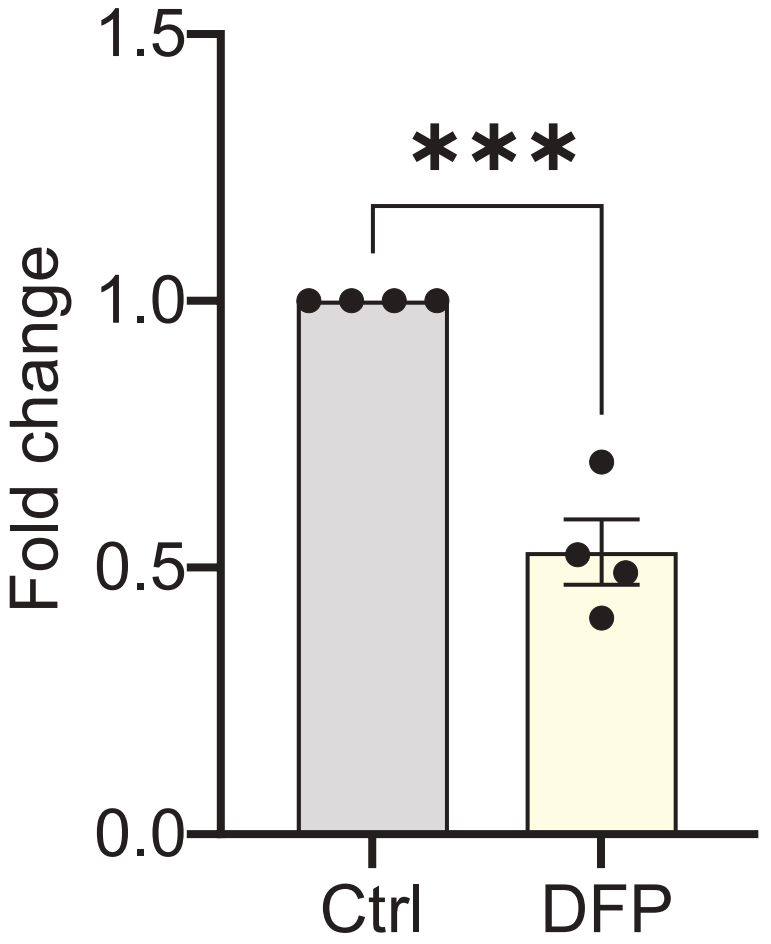

Supplementary Figure 8

Supplementary Figure 8. Deferiprone lowers macrophage total iron levels. Total iron as measured by graphite furnace atomic absorption spectrometry (GFAAS) in fetal liver-derived macrophages (FLAMs) treated with 24 hours of 100 μM of deferiprone (DFP) relative to control macrophages. Data presented mean ± SEM with p-value by unpaired Student's t test, ***p<0.001.

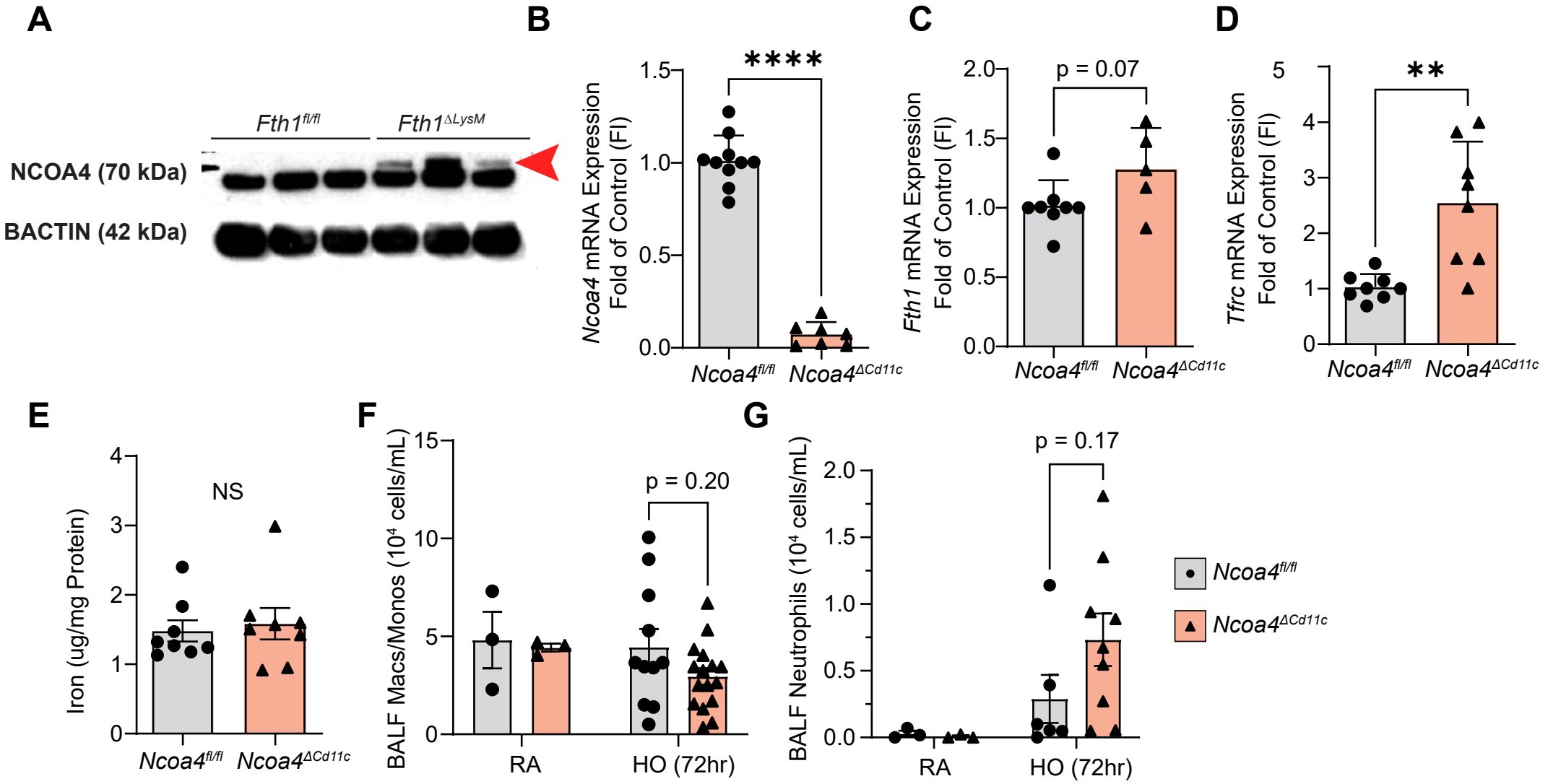

Supplementary Figure 9

Supplementary Figure 9. Alveolar macrophage (AM) NCOA4 depletion alters AM iron metabolism and cellular response to hyperoxia. (**A**) Representative immunoblot of NCOA4 protein expression in bone marrow-derived macrophages (BMDMs) from *Fth1*$^{fl/fl}$ (n=3) and *Fth1*$^{\Delta LysM}$ (n=3) mice; same membrane re-blotted as Figure 3B. Real-time polymerase chain reaction (RT-PCR) of AM *Ncoa4* (**B**, n=10 for *Ncoa4*$^{fl/fl}$, n=7 for *Ncoa4*$^{\Delta Cd11c}$), *Fth1* (**C**, n=8 for *Ncoa4*$^{fl/fl}$, n=5 for *Ncoa4*$^{\Delta Cd11c}$) and *Tfrc* (**D**, n=8 for *Ncoa4*$^{fl/fl}$, n=8 for *Ncoa4*$^{\Delta Cd11c}$) mRNA expression. (**E**) Total iron content in AMs from *Ncoa4*$^{fl/fl}$ and *Ncoa4*$^{\Delta Cd11c}$ mice, normalized to total protein. BALF macrophages/monocytes (**F**) and neutrophil count (**G**) in *Ncoa4*$^{fl/fl}$ and *Ncoa4*$^{\Delta Cd11c}$ mice under RA and hyperoxia conditions. Data (B-G) presented mean ± SEM with p-values by unpaired Student's t-test (B-E) or 2-way analysis of variance (ANOVA) with Šídák's correction (F-G) for multiple comparisons. **p<0.01, ****P<0.0001.

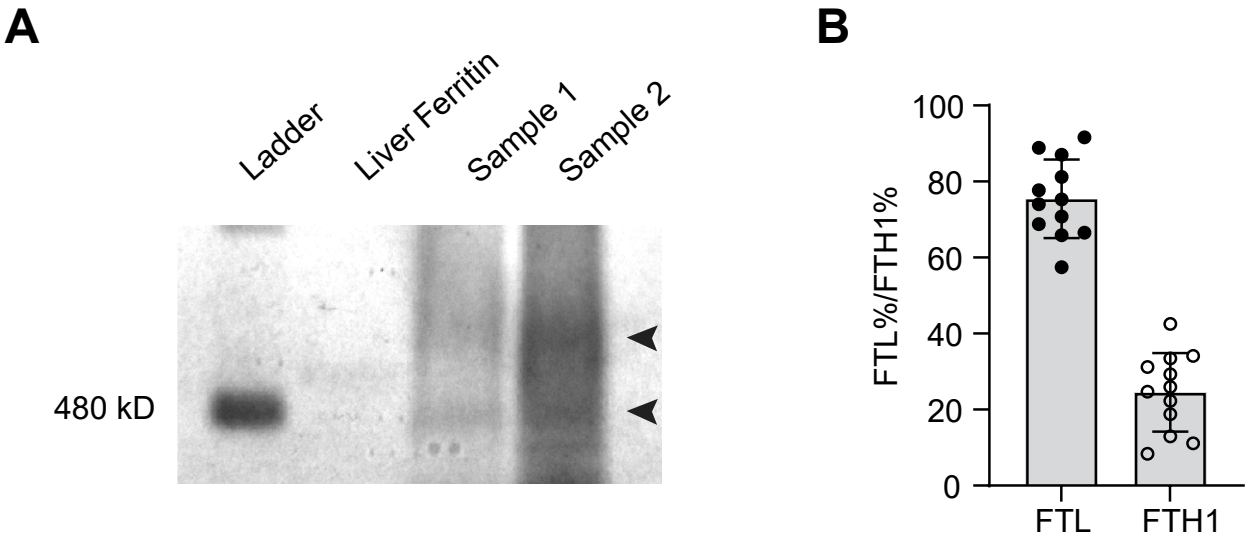

Supplementary Figure 10

Supplementary Figure 10. Serum ferritin in human ARDS is enriched for FTL. (**A**) Representative native electrophoresis gel image from native serum ferritin isolation, with quantification of FTL and FTH1 by mass spectrometry. (**B**) Relative percentage of FTL or FTH1 subunits.